

# Line-shape and poles of the $\psi(3770)$

Susana Coito<sup>a,1</sup>, Francesco Giacosa<sup>b,1,2</sup>

<sup>1</sup>Institute of Physics, Jan Kochanowski University, 25-406 Kielce, Poland

<sup>2</sup>Institut für Theoretische Physik, Johann Wolfgang Goethe-Universität, 60438 Frankfurt am Main, Germany

Received: date / Accepted: date

**Abstract** We study the non-Breit-Wigner line-shape of the  $\psi(3770)$  resonance, using an unitarized effective Lagrangian approach, including the one-loop effects of the nearby thresholds  $D^+D^-$  and  $D^0\bar{D}^0$ . The model contains a single seed state, corresponding to a standard  $\bar{c}c$  with predominant quantum numbers  $1\ ^3D_1$ . The loops of  $D^+D^-$  and  $D^0\bar{D}^0$  are responsible for the distortion of the spectral function. A fit of the theoretical data to the total cross-section  $e^+e^- \rightarrow D\bar{D}$  is performed with 28 data points and 4 parameters: strong and electromagnetic coupling constants, the bare mass of  $\psi(3370)$ , and a form-factor parameter, leading to a good description of data ( $\chi^2/\text{d.o.f.} \sim 0.86$ ). We then analyze various consequences of the fit, among which pole positions (which were not investigated in previous theoretical works), partial cross-sections, and leptonic decays. The first pole reads  $3777 - i12$  MeV, and it is in good agreement with the Particle Data Group (PDG) mass and width estimation for this state. Quite remarkably, there is also a second pole at  $3741 - i18$  MeV. This additional, dynamically generated, companion pole is responsible for the deformation of the left side of the line-shape. Its existence represents one of the main finding of this work. Moreover, the  $e^+e^- \rightarrow D^0\bar{D}^0$  and  $e^+e^- \rightarrow D^+D^-$  cross sections turn out to be separately in good agreement with data. The width for the decay  $\psi(3370) \rightarrow e^+e^-$  is 113 eV, hence smaller than the PDG fit of  $262 \pm 18$  eV, yet in agreement with a recent experimental study. Finally, the final state rescattering effect is found to be small. The size of the wavefunction is estimated within a Schrödinger model to be around 0.93 fm, a value that we relate to the form-factor of the effective field theoretical framework.

<sup>a</sup>e-mail: scoito@ujk.edu.pl

<sup>b</sup>e-mail: fgiacosa@ujk.edu.pl

## 1 Introduction

The  $\psi(3770)$  resonance is a vector state that was first detected at SPEAR [1] in 1977. The signal was fitted with a pure  $p$ -wave Breit-Wigner distribution, but with a not insignificant error ( $\chi^2 = 16.9$  for 15 degrees of freedom). More recently, the interest on this state was revived, and the parameters are nowadays fitted by the Particle Data group (PDG) as  $3773.13 \pm 0.35$  MeV for the mass and  $27.2 \pm 1.0$  MeV for the width [2]. According to the ‘quark model review’ of the PDG, the  $\psi(3770)$  resonance is classified as a  $1\ ^3D_1$  charmonium state, the first one above the  $D\bar{D}$  threshold, which is the reason for its relatively large width. Also for this reason, it is reasonable to expect, besides kinematic interference, additional nonperturbative effects.

Indeed, as stated above, the line shape of this resonance turned out to be quite anomalous. Although other experiments have been performed with observations in  $D\bar{D}$  channel [3,4,5,6,7], the deformation on the line-shape of the  $\psi(3770)$  was made clear by the BES Collaboration data in the  $e^+e^-$  annihilation to hadrons [8]. The existence of a second resonance was suggested, although possible dynamical effects, generated by the  $D\bar{D}$  threshold were not discarded. A deformation of a line-shape due to the superposition of two resonances has been discussed before e.g., for the scalar kaon [9], where, besides the dominant  $\bar{q}q$  state, an additional dynamically generated state arises from the continuum, the well known  $K_0^*(800)$ . Such effect has not been discussed before for the vector charmonium.

Various analysis of the  $\psi(3770)$  have been performed. In Refs. [10,11] fits were computed taking into account not only the  $D\bar{D}$  interference but also the tail of the  $\psi(2S)$ . Such inclusion is natural since the  $\psi(3770)$  should be a mixed state  $|1\ ^3D_1\rangle - |2\ ^3S_1\rangle$ . In Ref. [12], the de-

formation from the right side of the resonance, i.e. a dip structure, is explained by the interference with the  $D\bar{D}$  kinematical background which is higher for larger relative momentum. The same dip is reproduced in [10], using  $D\bar{D}$  background only, and in [13], where in addition, the continuum of light hadrons is removed. In [14] BES measured an unexpectedly large branching fraction  $\psi(3770) \rightarrow \text{non-}D\bar{D}$  of about 15%, a result that is not contradicted by CLEO in [15], within errors. Predictions for such non- $D\bar{D}$  continuum were made including the tails of  $J/\psi$  and  $\psi(2S)$ ,  $\tau\tau$  and  $uds$  decays [16], other excited  $\psi$  states [17], the  $D\bar{D}^*$  channel [18], other hadronic decays and radiative decays [11], and final state interactions [19], which in any case do not sum up to the value of 15%. Yet, since the phase space to  $D\bar{D}$  is not excessively large, it is likely that the missing decays are simply the sum of all the many Okubo-Zweig-Iizuka (OZI)-suppressed hadronic decays, that have not been studied systematically in the theory. Estimations for the  $\psi(3770)$  production via  $p\bar{p}$  annihilation are made in [20, 21, 22], which may possibly be measured at the PANDA experiment [23].

In this work, we study the properties of the  $\psi(3770)$  by analyzing its production through electron-positron fusion, and subsequent decay into  $D\bar{D}$  pairs (for a preliminary study, see Ref. [24]). Our starting point is a vector charmonium “seed” state, which gets dressed by “clouds” of  $D^+D^-$  and  $D^0\bar{D}^0$  mesons. Our aim is to study the deformation seen on the left side of the resonance in Ref. [8] with mesonic loops combined with the nearby thresholds. To this end, we use an effective relativistic Lagrangian approach in which a single vector state  $\psi \equiv \psi(3770)$  is coupled to  $D^+D^-$  and  $D^0\bar{D}^0$  as well as to lepton pairs. The propagator of  $\psi$  is calculated at the resummed one-loop level and fulfills unitarization requirements. Then, we perform a fit of the four parameters of our approach, i.e. the couplings of  $\psi$  to  $D\bar{D}$  and of  $\psi$  to leptons, the mass of  $\psi$ , and a cut-off responsible for the finite dimension of the  $\psi$  meson, to the experimental result of Refs. [6] and [4] for the cross-section of the reaction  $e^+e^- \rightarrow D\bar{D}$  in the energy region of about 20 MeV above the  $D^0\bar{D}^0$  threshold. We assume that the  $\psi(3770)$  resonance dominates in this energy range. We obtain a very good description of the data, which in turn allows us to determine in a novel and independent way the mass, width, and branching ratios of the  $\psi(3370)$ . Moreover, we study, to our knowledge for the first time, the poles of this state. Quite remarkably, we find *two* pole positions for this resonance, one which roughly corresponds to the peak of the resonance, the seed pole, and one additional dynamically generated pole, responsible for the enhancement left from the peak, which emerges due to the strong cou-

pling between the seed state and the mesonic loops. This is a companion pole, similarly to the one found in the kaonic system in Ref. [9]. (For other works on dynamically generated states in general and companion poles in particular, see Refs. [25, 9, 26, 27, 28, 29, 30, 31] and references therein).

As a consequence of the determined parameters, we also show that the cross sections  $e^+e^- \rightarrow D^+D^-$  and  $e^+e^- \rightarrow D^0\bar{D}^0$  agree separately to data. Being the resonance not an ideal Breit-Wigner one, different definitions for the partial widths are compared to each other. As a verification of our theoretical approach, we artificially vary the intensity of the coupling in order to show its effect on the line-shape of the resonance. Smaller couplings lead to a narrow Breit-Wigner shape, while larger couplings to an even larger deformation, which eventually gives rise to two peaks, as in Ref. [28]. In addition, we also test the role of the rescattering effect due to additional processes of the type  $D\bar{D} \rightarrow D\bar{D}$  (such rescattering partly mimics also the effect of the charmonium state below threshold  $\psi(2S)$ , otherwise not included in this work). We find that they affect only marginally the results. This is in agreement with one of the fits found in Refs. [32, 33], where effective Lagrangians including the  $\psi(2S)$ ,  $D\bar{D}$  loops, and rescattering have been employed.

The paper is organized as it follows. In Sec. 2 the model is introduced and various theoretical quantities, such as the resummed propagator, spectral function, cross-section, and rescattering, are presented. In Sec. 3 we show our results: first, we present a fit to data and then examine its consequences. In Sec. 4 conclusions are drawn. Some important technical details are discussed in the Appendices.

## 2 An Effective Model

In this section we present the Lagrangian of the model and evaluate the most relevant theoretical quantities, namely the resummed propagator and the spectral functions, needed to calculate the cross section for the processes  $e^+e^- \rightarrow D^+D^-$  and  $e^+e^- \rightarrow D^0\bar{D}^0$ , via production of the  $\psi(3770)$ , and with  $D^0\bar{D}^0 + D^+D^-$  one-loops, as represented in Fig. 1.

### 2.1 The strong Lagrangian and dispersion relations

We aim to write down a Lagrangian for the strong interaction between a single vectorial resonance and two pseudoscalar mesons. The bare resonance  $\psi \equiv \psi(3770)$  is identified with a bare quarkonium  $c\bar{c}$  state, with predominant quantum numbers  $N^{2S+1}L_J = 1^3D_1$ , but

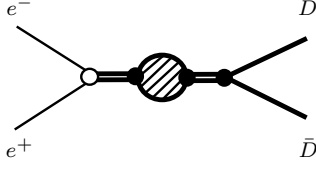


**Fig. 1** Reaction  $e^- e^+ \rightarrow \psi(3770) \rightarrow D\bar{D}$  with  $D^0\bar{D}^0 + D^+D^-$  loops (cf. Fig. 3).

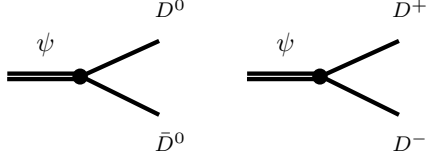


**Fig. 2** Interaction vertices  $\psi \rightarrow D^0\bar{D}^0$  and  $\psi \rightarrow D^+\bar{D}^-$ , corresponding to the Lagrangian in Eq. (1).

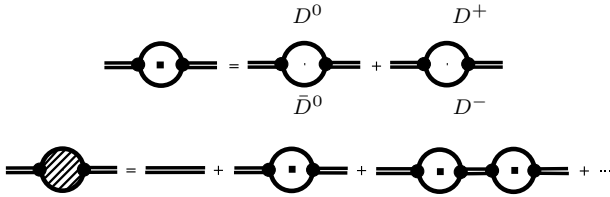


**Fig. 3** Upper diagram: one-loop  $D\bar{D} = D^0\bar{D}^0 + D^+D^-$ . Lower diagram: Full one-loop expansion (cf. Fig. 1).

admixtures of other quantum numbers, most notably the  $2^3S_1$ , are possible. In our model, however, neither the quarkonium structure nor the orbital angular momentum mixing are explicit, since we work with mesonic degrees of freedom in the basis of total angular momentum. The effective strong Lagrangian density, for the charmonium state  $\psi$ , reads

$$\mathcal{L}_{\psi D\bar{D}} = ig_{\psi D^0\bar{D}^0}\psi_\mu \left( \partial^\mu D^0\bar{D}^0 - \partial^\mu \bar{D}^0 D^0 \right) + ig_{\psi D^+D^-}\psi_\mu \left( \partial^\mu D^+D^- - \partial^\mu D^-D^+ \right), \quad (1)$$

which corresponds to the simplest interaction among  $\psi$  and its main decay products, the pseudoscalar pairs  $D^0\bar{D}^0$  and  $D^+D^-$ , each vertex represented in Fig. 2. In this work, we shall take into account the small mass difference between  $D^0$  and  $D^+$ , i.e. isospin breaking for the masses, but shall keep the same coupling constant, i.e. isospin symmetry for the decays, and we define  $g_{\psi D^0\bar{D}^0} = g_{\psi D^+D^-} \equiv g_{\psi D\bar{D}}$ . The full Lagrangian can be found in Appendix A.

The free propagator of a vector field  $\psi$ , with mass  $m_\psi$  and momentum  $p$ , is given by

$$G_{\mu\nu}(p) = \frac{1}{p^2 - m_\psi^2 + i\varepsilon} \left( -g_{\mu\nu} + \frac{p_\mu p_\nu}{m_\psi^2} \right), \quad (2)$$

where the term in parenthesis is the sum over the three polarization states of a vector. We include the resummed one-loop effect as shown in Fig. 3, leading to the full propagator of  $\psi$

$$\Delta_{\mu\nu}(p) = G_{\mu\nu}(p) + G_{\mu\mu'}(p)\Pi_{\mu'\nu'}(p)G_{\nu'\nu}(p) + \dots, \quad (3)$$

where  $\Pi_{\mu\nu}(p)$  is the loop-function, consisting of two contributions, the  $D^0\bar{D}^0$  loops and the  $D^+D^-$  loops. In particular, we get

$$\Pi_{\mu\nu}(p) = g_{\psi D\bar{D}}^2 \{ \Sigma_{\mu\nu}(s, m_{D^0}) + \Sigma_{\mu\nu}(s, m_{D^+}) \}, \quad (4)$$

where the function  $\Sigma_{\mu\nu}(s, m)$ , with  $\int_q \equiv \int \frac{d^4 q}{(2\pi)^4}$ , reads

$$\Sigma_{\mu\nu}(s, m) = i \times \int_q \frac{4 q_\mu q_\nu f_A^2(s)}{[(q+p/2)^2 - m^2 + i\varepsilon][(q-p/2)^2 - m^2 + i\varepsilon]}, \quad (5)$$

where  $m$  is the mass of the meson circulating in the loop (either  $D^0$  or  $D^+$ ), and  $q$  is the internal momentum of the loop. Note, in the reference frame of the decaying particle, it holds the relation

$$s = p^2 = E^2, \quad p = (E, \mathbf{0}). \quad (6)$$

An important element for our discussion is the function  $f_A(s)$  entering in Eq. (5). This is a form-factor that depends on a cutoff parameter  $\Lambda$  and on the invariant energy squared  $s$ . It is needed to account for the unknown of the black vertices in Fig. 2, due to the fact that mesons are not elementary particles [26]. The cutoff function must ensure the convergence of the integral. We choose the following Gaussian form

$$f_A(s) = e^{-s/(4\Lambda^2)} \times e^{(m_{D^0}^2 + m_{D^+}^2)/(2\Lambda^2)}, \quad (7)$$

where the second term is built for convenience (in the isospin limit,  $f_A$  reduces to  $e^{-k^2/\Lambda^2}$ , being  $k$  the relativistic momentum of the final state). One can formally introduce the vertex function already at the Lagrangian level by rendering it nonlocal, see the discussion in Refs. [34, 35, 36, 26], where it is also pointed out that the special form of the form factor is not important, as long as fast convergence is guaranteed. However, the exponential form for the cutoff is very typical and has been used in many different approaches in hadron physics, e.g. Ref. [35]. Finally, as shown in Ref. [37], covariance can be always guaranteed when introducing the form factor.

We now turn back to the study of the propagator. In Appendix B, it is shown that the relevant quantity is the transverse part of the propagator that, in the rest

frame of the decaying particles, and for a single loop, reads

$$\begin{aligned}\Sigma(s, m) &= \frac{1}{3} \left( -g^{\mu\nu} + \frac{p^\mu p^\nu}{p^2} \right) \Sigma_{\mu\nu}(s, m) \\ &= -\frac{i}{3} \int_q \frac{4 \mathbf{q}^2 f_A^2(s)}{[(q + \frac{p}{2})^2 - m^2 + i\varepsilon][(q - \frac{p}{2})^2 - m^2 + i\varepsilon]},\end{aligned}\quad (8)$$

and similarly for the sum

$$\begin{aligned}\Pi(s) &= \frac{1}{3} \left( -g^{\mu\nu} + \frac{p^\mu p^\nu}{p^2} \right) \Pi_{\mu\nu}(s) \\ &= g_{\psi D \bar{D}}^2 \{ \Sigma(s, m_{D^0}) + \Sigma(s, m_{D^+}) \}.\end{aligned}\quad (9)$$

The scalar part of the one-loop resummed dress propagator (see Appendix B for details) reads

$$\Delta(s) = \frac{1}{s - m_\psi^2 + \Pi(s)}. \quad (10)$$

Note, this expression of the propagator fulfills unitarity (cf. Sec. 2.4 below) and it is accurate as long as further contributions to the self-energy are small. The next contribution would be represented by a loop in which the unstable state  $\psi$  would be exchanged by  $D$  mesons circulating in the loop. Indeed, as shown in Ref. [38], such contributions are typically very small in hadron physics and can be safely neglected.

The self-energy in Eq. (5) can either be computed through the integration (see Appendix B), or using dispersion relations. We follow the latter. To this end, we first decompose  $\Sigma(s, m)$  into its real and imaginary parts

$$\Sigma(s, m) = R(s, m) + iI(s, m), \quad R, I \in \mathbb{R}. \quad (11)$$

According to the optical theorem, the imaginary part  $I(s, m)$  (dispersive term) is given by

$$I(s, m) = \frac{k(s, m)}{8\pi\sqrt{s} g_{\psi D \bar{D}}^2} |\mathcal{M}_{\psi \rightarrow D \bar{D}}|^2, \quad (12)$$

with  $k(s, m) = \sqrt{s/4 - m^2}$  being the center-of-mass momentum. The partial decay widths of  $\psi \rightarrow D^0 \bar{D}^0$  and  $\psi \rightarrow D^+ D^-$  are, then, calculated as

$$\begin{aligned}\Gamma_{\psi \rightarrow D^0 \bar{D}^0}(s) &= \frac{k(s, m_{D^0})}{8\pi s} |\mathcal{M}_{\psi \rightarrow D^0 \bar{D}^0}|^2 \\ &= g_{\psi D \bar{D}}^2 \frac{I(s, m_{D^0})}{\sqrt{s}},\end{aligned}\quad (13)$$

$$\begin{aligned}\Gamma_{\psi \rightarrow D^+ D^-}(s) &= \frac{k(s, m_{D^+})}{8\pi s} |\mathcal{M}_{\psi \rightarrow D^+ D^-}|^2 \\ &= g_{\psi D \bar{D}}^2 \frac{I(s, m_{D^+})}{\sqrt{s}},\end{aligned}\quad (14)$$

where the Lorentz invariant amplitudes squared, computed from  $\mathcal{L}_I$  in Eq. (1), are given by

$$|\mathcal{M}_{\psi \rightarrow D^0 \bar{D}^0}|^2 = g_{\psi D \bar{D}}^2 \frac{4}{3} k^2(s, m_{D^0}) f_A^2(s), \quad (15)$$

$$|\mathcal{M}_{\psi \rightarrow D^+ D^-}|^2 = g_{\psi D \bar{D}}^2 \frac{4}{3} k^2(s, m_{D^+}) f_A^2(s). \quad (16)$$

Finally, the on-shell partial and total decay widths are

$$\Gamma_{\psi \rightarrow D^0 \bar{D}^0}^{\text{on-shell}} = \Gamma_{\psi \rightarrow D^0 \bar{D}^0}(m_\psi^2), \quad (17)$$

$$\Gamma_{\psi \rightarrow D^+ D^-}^{\text{on-shell}} = \Gamma_{\psi \rightarrow D^+ D^-}(m_\psi^2), \quad (18)$$

$$\Gamma_{\psi \rightarrow D \bar{D}}^{\text{on-shell}} = \Gamma_{\psi \rightarrow D^0 \bar{D}^0}^{\text{on-shell}} + \Gamma_{\psi \rightarrow D^+ D^-}^{\text{on-shell}}. \quad (19)$$

Once the imaginary part of the loop is known, the real part, the function  $R(s, m)$ , is computed from the dispersion relation

$$R(s, m) = \frac{PP}{\pi} \int_{s_{th}=4m^2}^{\infty} \frac{I(s', m)}{s' - s} ds', \quad (20)$$

where  $I(s', m)$  is zero below threshold. Convergence is guaranteed by the cutoff function. As we shall see in Sec. 3, the real part  $R(s, m)$  causes a distortion in the line-shape due to the continuous shifting of the physical mass of the resonance with the energy. Note, when the energy  $E = z$  is complex, the function  $\Sigma(s = z^2, m)$  reads (away from the real axis):

$$\Sigma(z^2, m) = \frac{1}{\pi} \int_{s_{th}=4m^2}^{\infty} \frac{I(s', m)}{s' - z^2} ds'. \quad (21)$$

Furthermore, although it is not strictly needed, since the integral in Eq. (20) is already convergent, we use the once-subtracted dispersion relation, with subtraction in point  $m_\psi^2$ , for our convenience. Hence, the total loop-function is given by

$$\Pi_1(s) = \Pi(s) - R(m_\psi^2, m_{D^0}) - R(m_\psi^2, m_{D^+}), \quad (22)$$

and, the final dressed propagator of meson  $\psi$  is

$$\Delta(s) = \frac{1}{s - m_\psi^2 + \Pi_1(s)}. \quad (23)$$

In this way, the parameter  $m_\psi$  in the propagator corresponds to the mass of the particle defined as

$$\text{Re } \Delta_\psi(s)^{-1} = 0 \rightarrow s = m_\psi^2. \quad (24)$$

Other definitions for the mass are possible, such as the position of the peak, or the real part of the pole, as we shall see below.

## 2.2 Poles

In order to find poles, the energy  $E$  is analytically continued to the complex plane ( $E \rightarrow z$ ). In case of two decay channels, the Riemann surface is composed by four Riemann Sheets (RSs). Poles are found in the unphysical sheet which results in the physical sheet when the energy is real and the resonance can be seen. Above both thresholds, this corresponds to the condition  $\text{Im } k_{D^0} < 0$  and  $\text{Im } k_{D^+} < 0$  when  $\text{Re } E > 2m_{D^0}$  and  $\text{Re } E > 2m_{D^+}$ , i.e., the fourth RS. Poles are given when the denominator of the propagator in Eq. (23) is zero in the correct RS, i.e.,

$$z^2 - m_\psi^2 + \Pi_{1,IV}(z^2) = 0, \quad z \in \mathbb{C}, \quad (25)$$

where

$$\begin{aligned} \Pi_{1,IV}(z^2) &= \Pi_{1,I}(z^2) \\ &- 2ig_{\psi D\bar{D}}^2[I_I(z^2, m_{D^0}) + I_I(z^2, m_{D^+})] = 0, \end{aligned} \quad (26)$$

where the subscripts  $I$  and  $IV$  stand for the first and fourth RS.

## 2.3 Coupling to leptons

The available experimental data comes from the production process  $e^+e^- \rightarrow \psi \rightarrow D\bar{D}$  (see Fig. 1), therefore we need to couple the state  $\psi(3370)$  to leptons. The corresponding interaction Lagrangian is defined by

$$\mathcal{L}_{\psi l^+l^-} = g_{\psi e^+e^-} \psi_\mu \sum_{l=e,\mu,\tau} \Psi_{l^+} \gamma^\mu \Psi_{l^-}, \quad (27)$$

which is the simplest interaction among a massive vector field  $\psi$  and a fermion-antifermion pair. The coupling  $g_{\psi e^+e^-}$ , between  $\psi$  and the electron-positron pair, is here considered to be the same between  $\psi$  and all leptonic pairs, and it is the overall strength for the annihilation of the leptonic pair  $l^+l^-$  into one photon, and further conversion into the  $\psi$  vector. For our purposes, it is more convenient to enclose this process in a single effective vertex  $e^-e^+ \rightarrow \psi$ , see Fig. 4.

The corresponding decay into leptons reads

$$\Gamma_{\psi \rightarrow l^+l^-}(s) = \frac{p_l(s)}{8\pi s} \frac{4}{3} (s + 2m_l^2) g_{\psi e^+e^-}^2, \quad (28)$$

where  $m_l$  is the leptonic mass. In principle, the loops of leptons should be included in the total one-loop function of resonance  $\psi(3370)$ , obtaining  $\Pi_{tot}(s) = \Pi(s) + \sum_l \Pi_l(s) + \dots$ , where dots refer to other possible but suppressed hadronic decay channels. However, the loop contribution of  $\Pi_l(s)$  is definitely negligible w.r.t.  $\Pi(s)$ . Here, we shall simply consider  $\Pi_{tot}(s) = \Pi(s)$ .

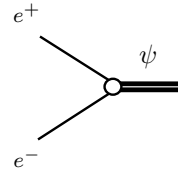


Fig. 4 Interaction vertex  $e^-e^+ \rightarrow \psi(3370)$ .

## 2.4 Spectral function and cross section

The unitarized spectral function, as a function of energy  $E$ , equivalent to the running mass of the  $\psi(3370)$  resonance, is given by

$$\begin{aligned} d_\psi(E) &= -\frac{2E}{\pi} \text{Im } \Delta(E) \\ &= \frac{2E^2}{\pi} \frac{\Gamma_{\psi \rightarrow D^0\bar{D}^0}(E^2) + \Gamma_{\psi \rightarrow D^+\bar{D}^-}(E^2)}{[E^2 - m_\psi^2 + \text{Re } \Pi_1(E^2)]^2 + [\text{Im } \Pi_1(E^2)]^2}, \end{aligned} \quad (29)$$

that has the general shape of a relativistic Breit-Wigner distribution, distorted by the loop-function  $\Pi_1$  (Eq. (22)). When no poles below threshold emerge, the normalization above threshold is guaranteed (unitarity):

$$\int_{2m_{D^0}}^{\infty} d_\psi(E) dE = 1. \quad (30)$$

The quantity  $d_\psi(E)dE$  is interpreted as the probability that the state  $\psi(3370)$  has a mass between  $E$  and  $E + dE$ . The cross section for  $e^+e^- \rightarrow D\bar{D} = D^+D^- + D^0\bar{D}^0$  takes the form

$$\sigma_{e^+e^- \rightarrow D\bar{D}} = \frac{\pi}{2E} g_{\psi e^+e^-}^2 d_\psi(E) = -g_{\psi e^+e^-}^2 \text{Im } \Delta(E). \quad (31)$$

Hence, the experimental data for this cross section give us direct access to the imaginary part of the propagator of the meson  $\psi(3370)$ . The corresponding amplitude, leading to  $\sigma_{e^+e^- \rightarrow D\bar{D}}$ , is depicted in Fig. 1.

One also defines the partial spectral functions [39]:

$$\begin{aligned} d_{\psi \rightarrow D^+D^-}(E) &= \frac{2E^2}{\pi} \times \\ &\frac{\Gamma_{\psi \rightarrow D^+D^-}(E^2)}{[E^2 - m_\psi^2 + \text{Re } \Pi_1(E^2)]^2 + [\text{Im } \Pi_1(E^2)]^2}, \end{aligned} \quad (32)$$

$$\begin{aligned} d_{\psi \rightarrow D^0\bar{D}^0}(E) &= \frac{2E^2}{\pi} \times \\ &\frac{\Gamma_{\psi \rightarrow D^0\bar{D}^0}(E^2)}{[E^2 - m_\psi^2 + \text{Re } \Pi_1(E^2)]^2 + [\text{Im } \Pi_1(E^2)]^2}. \end{aligned} \quad (33)$$

Intuitively,  $d_{\psi \rightarrow D^+D^-}(E)dE$  is the probability that the unstable state  $\psi(3370)$  has a mass between  $E$  and  $E + dE$  and decays in the channel  $D^+D^-$  (similarly for



**Fig. 5** Full propagator, including  $D\bar{D}$  loops (cf. Fig. 2) and  $D\bar{D}$  rescattering.

$d_{\psi \rightarrow D^0 \bar{D}^0}(E)$ ). Then, the partial cross sections are given by:

$$\sigma_{e^+e^- \rightarrow D^+D^-} = \frac{\pi}{2E} g_{\psi e^+e^-}^2 d_{\psi \rightarrow D^+D^-}(E), \quad (34)$$

$$\sigma_{e^+e^- \rightarrow D^0 \bar{D}^0} = \frac{\pi}{2E} g_{\psi e^+e^-}^2 d_{\psi \rightarrow D^0 \bar{D}^0}(E), \quad (35)$$

$$\sigma_{e^+e^- \rightarrow D\bar{D}} = \sigma_{e^+e^- \rightarrow D^+D^-} + \sigma_{e^+e^- \rightarrow D^0 \bar{D}^0}. \quad (36)$$

## 2.5 Rescattering

For completeness, we also study the possibility of final state rescattering, that takes place by additional processes of the type  $D\bar{D} \rightarrow D\bar{D}$ , see Fig. 5. Formally, the interaction Lagrangian responsible for the rescattering reads

$$\mathcal{L}_{D\bar{D}}^{\text{resc}} = \lambda \left( \partial^\mu D^0 \bar{D}^0 - \partial^\mu \bar{D}^0 D^0 \right)^2 \quad (37)$$

$$+ \lambda \left( \partial^\mu D^+ D^- - \partial^\mu D^- D^+ \right)^2. \quad (38)$$

where  $\lambda$  is an additional rescattering coupling parameter. Note, such rescattering effect includes various  $t$ -meson exchanges between  $D\bar{D}$ , and also  $s$ -channel exchanges of nearby vector resonances, such as  $\psi(2S)$ , due to the chain  $D\bar{D} \rightarrow \psi(2S) \rightarrow D\bar{D}$ . Figure 5 depicts the rescattering effect over the loop function. The filled square is the total self-energy, including the rescattering expansion, and reads explicitly:

$$\tilde{\Pi}^{\text{resc}}(s) = \Pi + \Pi \lambda \Pi + \dots = \Pi \sum_{n=0} (\lambda \Pi)^n = \frac{\Pi(s)}{1 - \lambda \Pi(s)}, \quad (39)$$

The once-subtracted technique may be employed to redefine the self-energy in Eq. (39), in a similar way to Eq. (22). This can be done in two different ways

$$\tilde{\Pi}_1^{\text{resc}}(s) = \Pi_1(s) / (1 - \lambda \Pi_1(s)), \quad (40)$$

where the subtraction is applied to each loop, and

$$\tilde{\Pi}_{\psi,2}^{\text{resc}}(s) = \tilde{\Pi}^{\text{resc}}(s) - \text{Re } \tilde{\Pi}^{\text{resc}}(m_\psi^2), \quad (41)$$

where the subtraction constant is applied over the whole self-energy without subtractions. In either way, we shall show that reasonable choices of  $\lambda$  lead to small variation of the spectral function, hence for the state  $\psi(3370)$ , rescattering effects seem to play a minor role.

$m_\psi$ (MeV)	$3773.05 \pm 0.95$
$\Lambda$ (MeV)	$30.7 \pm 4.8$
$g_{\psi D\bar{D}}$	$272.55 \pm 1.17$
$g_{\psi e^+e^-}$	$(1.062 \pm 0.032) \times 10^{-3}$
$\chi^2$	20.52
$\chi^2/d.o.f$	0.86

**Table 1** Fitting parameters.

## 3 Line-shapes, poles, and wave-function

In this section, we present our fit to experimental data and its consequences, most notably the position of two poles underlying  $\psi(3370)$ . We also discuss the spatial dimension of the resonance.

### 3.1 Fit to data and consequences

As a first necessary step, we determine the four free parameters of our model defined in Sec. 2,

$$\{g_{D\bar{D}}, m_\psi, \Lambda, g_{\psi e^+e^-}\}, \quad (42)$$

by performing a fit to the cross section data for the process  $e^+e^- \rightarrow \psi \rightarrow D\bar{D} = D^0 \bar{D}^0 + D^+ D^-$ . We use 28 experimental points published in Refs. [6] and [4], and the theoretical expression in Eq. (31). The fit to data is shown in Fig. 6, and the values of the parameters in (42) are presented in Table 1. We get the value  $\chi^2/d.o.f. \simeq 0.86$ , which shows that a very good description of the data is achieved. The errors of the parameters can be obtained in the standard way. Usually, the error  $\delta x$  of a parameter  $x$  corresponds to an increase of the unity of the  $\chi^2$  (see e.g. Ref. [45]). Yet, being the  $\chi^2/d.o.f. < 1$ , we take here a more conservative determination by increasing the errors by the multiplicative factor  $\sqrt{(d.o.f. - \chi^2 + 1)}$  (hence, we take into account that a larger departure from the value at the minimum is still compatible with the data).

There are various consequences of the fit that we discuss in detail:

a) The value of the mass  $m_\psi = 3773.05 \pm 0.95$  MeV (corresponding to the zero of the real part of the inverse's propagator, see Eq. (24)) is in well agreement with the present PDG fit of  $3773.13 \pm 0.35$  MeV [2].

b) In Fig. 7 we present a comparison between theory and the data for the cross sections  $\sigma_{e^+e^- \rightarrow D^+D^-}$  and  $\sigma_{e^+e^- \rightarrow D^0 \bar{D}^0}$ , using the parameters in Table 1. The

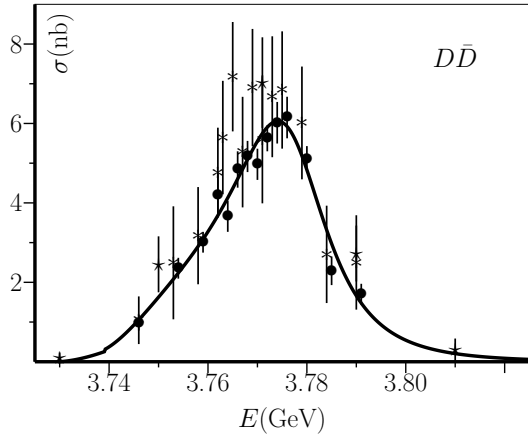


**Fig. 6** Data: • BES [6], \* BES [4], \* BaBar [5] (the latter not used in the fit). Solid line: our fit (cf. Table 1).

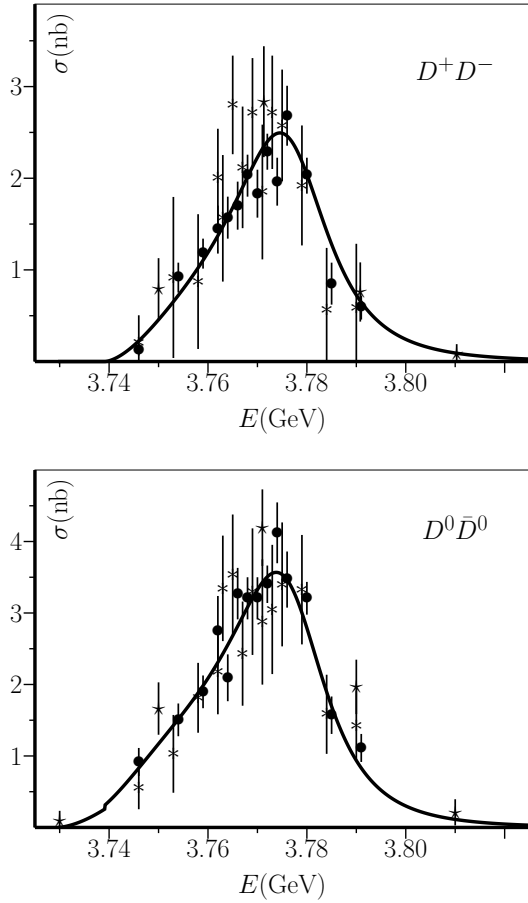


**Fig. 7** Data: • BES [6], \* BES [4], \* BaBar [5]. Solid line: our result, using the parameters in Table 1.

	$\Gamma(m_\psi^2)$	$\Gamma^{\text{average}}$
$\Gamma_{D^0 \bar{D}^0}$ (MeV)	$11.6 \pm 1.2$	10.87
$\Gamma_{D^+ D^-}$ (MeV)	$8.0 \pm 0.8$	6.94
$\Gamma_{D \bar{D}}$ (MeV)	$19.5 \pm 2.0$	17.82
$(\Gamma_{D^0 \bar{D}^0} / \Gamma_{D^+ D^-})$	1.45	1.57
$(\Gamma_{D^0 \bar{D}^0} / \Gamma_{D \bar{D}})$	0.59	0.61
$(\Gamma_{D^+ D^-} / \Gamma_{D \bar{D}})$	0.41	0.39

**Table 2** Decay widths and branching ratios using Eqs. (17)-(19), for the on-shell widths, and Eqs. (43)-(45), for the average widths.

good agreement shows that the theory is able to describe the two partial cross sections separately, without the need of some extra parameter.

c) The branching ratios and partial and total ( $D\bar{D}$ ) widths are presented in Table 2. The partial widths, evaluated on-shell, are defined in Eqs. (17)-(19). The branching ratios are in rough agreement with those quoted in PDG, but the total  $D\bar{D}$  three-level width is sizably smaller than the one referred in PDG which includes all decay channels. The ratio  $\Gamma_{\psi \rightarrow D^0 \bar{D}^0}^{\text{on-shell}} / \Gamma_{\psi \rightarrow D^+ D^-}^{\text{on-shell}}$  of 1.45 is compatible with the PDG values, which range from 1.04 to 1.51. However, as shown in Fig. 7, the functions  $\Gamma_{\psi \rightarrow D^0 \bar{D}^0}(E)$  and  $\Gamma_{\psi \rightarrow D^+ D^-}(E)$  strongly vary in the region of interest. Alternatively, one may use a different definition, cf. [26], to obtain the partial decay widths and the full decay width to  $D\bar{D}$ , by integrating over the spectral function as

$$\Gamma_{\psi \rightarrow D^0 \bar{D}^0}^{\text{average}} = \int_{2m_{D^0}}^{\infty} \Gamma_{\psi \rightarrow D^0 \bar{D}^0}(E^2) d_\psi(E) dE, \quad (43)$$

$$\Gamma_{\psi \rightarrow D^+ D^-}^{\text{average}} = \int_{2m_{D^+}}^{\infty} \Gamma_{\psi \rightarrow D^+ D^-}(E^2) d_\psi(E) dE, \quad (44)$$

$$\Gamma_{\psi \rightarrow D\bar{D}}^{\text{average}} = \Gamma_{\psi \rightarrow D^0 \bar{D}^0}^{\text{average}} + \Gamma_{\psi \rightarrow D^+ D^-}^{\text{average}}. \quad (45)$$

The distributions  $\Gamma_{D^0 \bar{D}^0}$  and  $\Gamma_{D^+ D^-}$  are depicted in Fig. 8 where, in addition, one can see clearly the effect of the cutoff.

A somewhat naive but still useful alternative determination of the mass is the value corresponding to the peak and the half-height width:

$$\begin{aligned} m_\psi^{\text{peak}} &\simeq 3785.0 \pm 1.0 \text{ MeV}, \\ I_{\psi \rightarrow D\bar{D}}^{\text{half-height}} &\simeq 21.7 \pm 2.0 \text{ MeV}, \end{aligned} \quad (46)$$

where we estimated the error of the peak mass as  $\sim 1$  MeV, close to the determined error for the parameter  $m_\psi$ , and the error of the distribution width as  $\sim 2$  MeV, coincident to the error for  $\Gamma_{D\bar{D}}$  (see Table 2). These

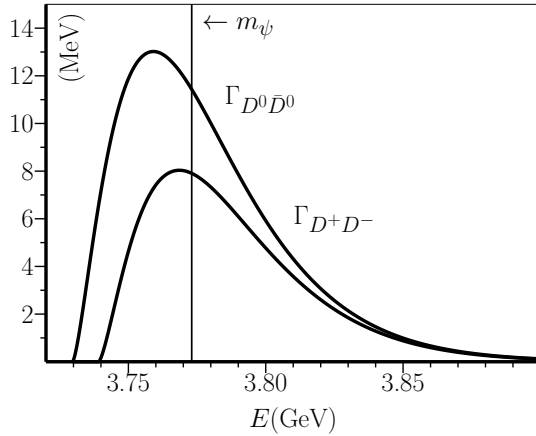


**Fig. 8** Partial widths using the cutoff function in Eq. (7), using parameters in Table 1. The width  $\Gamma_{D\bar{D}}$  is the sum of the width in each channel.

evaluations show that the resonance  $\psi(3770)$  is far from being an ideal Breit-Wigner. Namely, all these different approaches coincide for states with a very small width. Here, the distortions are sizable, hence clear definition of mass and width, as well as branching ratios, are difficult. A commonly used approach to get a uniform result, makes use of poles in the complex plane, as we show below.

d) Pole positions. As renowned, a theoretically (and lately experimentally as well, see e.g. the  $f_0(500)$  in PDG) stable approach to describe unstable states is based on the determination of the position of the corresponding poles. In the present case, one obtains, quite remarkably, two poles on the IV Riemann Sheet. As seen in Sec. 2.2, this is the sheet relevant for a system with two decay channels at energy above both thresholds. In the isospin limit, the IV RS reduces to the usual II RS. In the following, the indeterminacy of the pole masses is estimated to be  $\sim 1.0$  MeV, close to the error obtained for the parameter  $m_\psi$ , and the indeterminacy of the pole width(s) as  $\sim 2.0$  MeV, coincident with the error for  $\Gamma_{D\bar{D}}$  (see Table 2). In fact, the errors of these strictly correlated quantities must have a similar magnitude. The closest pole to the Riemann axis reads:

$$\text{First pole: } E = 3776.8 - i12.3 \text{ MeV,} \quad (47)$$

hence

$$\begin{aligned} m_\psi^{\text{pole}} &\simeq 3776.8 \pm 1.0 \text{ MeV and} \\ \Gamma_\psi^{\text{pole}} &\simeq 24.6 \pm 2.0 \text{ MeV,} \end{aligned} \quad (48)$$

$\Gamma_{e^+e^-}$ (eV)	$\Gamma_{\mu^+\mu^-}$ (eV)	$\Gamma_{\tau^+\tau^-}$ (eV)
$112.8 \pm 6.8$	$112.8 \pm 6.8$	$54.7 \pm 3.3$

**Table 3** Leptonic widths computed with Eq. (28).

which agrees quite well with the PDG values [2]. This pole is closely related to the seed charmonium state and to the position and width of the peak. Furthermore, a second broader pole appears at lower energy:

$$\text{Second pole: } E = 3741.2 - i18.5 \text{ MeV.} \quad (49)$$

This pole is *dynamically generated*, and it is related to the deformation of the signal on the left side. It is also referred to as a companion pole emergent due to the strong dynamics. The situation is very much reminiscent of the light scalar  $\kappa$  state at lower energy, which was interpreted as a dynamically generated companion pole of  $K_0^*$  in Ref. [37]. For additional recent works on this state, see Refs. [40, 41], and references therein.

e) The coupling  $g_{\psi e^+e^-}$  is an outcome of our fit, then the widths  $\Gamma_{\psi \rightarrow l^+l^-}$  can be easily computed from Eq. (28). Results are shown in Table 3. The value for  $\Gamma_{\psi \rightarrow e^+e^-}$  is smaller than the one given by PDG fit of  $262 \pm 18$  eV by a factor two, but it is compatible with the analysis in Ref. [7], that gives  $154^{+79+21}_{-58-27}$  eV. However, the mismatch of our result with the PDG estimate, that nevertheless lists a quite broad range of values from different experiments, shows that this decay rate should be further investigated in the future. Also the experimental identification of the decays into  $\mu^+\mu^-$  and  $\tau^+\tau^-$  could help to distinguish among different theories.

f) In our fit, we consider only the  $\psi(3370)$  resonance as a virtual state of the process  $e^+e^- \rightarrow D\bar{D}$ . As discussed above, a possible mixing between bare  $c\bar{c}$  states with quantum numbers  $1^3D_1$  and  $2^3S_1$  is automatically taken into account in our bare field  $\psi$  entering into the Lagrangian defined in Eq. (1). Indeed, the bare field, i.e., the field prior to the dressing by mesonic loops, represents the diagonal quark-antiquark state, while the  $\psi(3770)$  is a mixture of  $1^3D_1$  and  $2^3S_1$  configurations, with the  $\psi(2S)$  as its orthogonal state. Moreover, the effect of  $\psi(2S)$  can be taken into account through rescattering (see next subsection). Yet, the role of the  $\psi(2S)$  as an additional exchange in the reaction  $e^+e^- \rightarrow \psi(2S) \rightarrow D\bar{D}$  was not taken into account. Being  $\psi(2S)$  off-shell in the energy of interest, the propagator is expected to suppress this amplitude; moreover, also its coupling to channel  $D\bar{D}$  is expected to be small, due to the form-factor. Indeed, in Refs. [32, 33], the  $\psi(2S)$ ,  $D\bar{D}$  loops, and  $D\bar{D}$  rescattering have

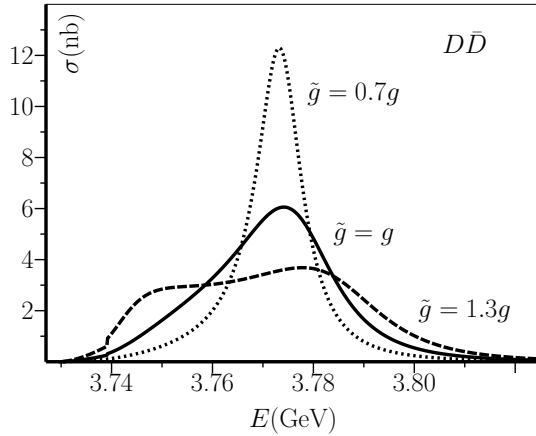


**Fig. 9** Variation of the cross section in channel  $D\bar{D}$  with the coupling  $\tilde{g}$ . Here,  $g \equiv g_{D\bar{D}} = 30.67$ , and the other parameters are found in Table 1. See corresponding poles in Table 4.

been considered, leading to two fits that are in good agreement with one of the experiments (Ref. [6]). In one of the fits the  $\psi(2S)$  contribution is very small, in agreement with our results. On the contrary, a second fit with a sizable role of  $\psi(2S)$ , has also been found. Our results strongly favor the first fit of Ref. [6]. Note, in Refs. [32, 33] the pole structure was not examined.

### 3.2 Variation of the coupling and rescattering

First, we study the effect of varying the coupling constant  $g_{\psi D\bar{D}}$ . Results are shown in Fig. 9 for the cross-section, and in Table 4 for pole positions. In Quantum Chromodynamics (QCD), a change in such coupling is equivalent to vary the number of colors according to the scaling  $g_{\psi D\bar{D}} \propto N_c^{-1/2}$ . As expected, a smaller value  $g_{\psi D\bar{D}}$  leads to a Breit-Wigner-like shape. While the first pole gets closer to the real axis, the second pole moves deeper in the complex plane and approaches the  $D^+D^-$  threshold. For a certain critical value, in this case  $g_{\psi D\bar{D}} < 26.9$ , the second pole completely disappears. On the contrary, increasing  $g_{\psi D\bar{D}}$  implies that the first pole runs away from the real axis, while the second pole approaches it. Eventually, the dynamically generated pole can get even closer to the real axis than the seed pole.

Finally, it is interesting to study the final-state rescattering, which we show in Fig. 10. It depends on the rescattering coupling  $\lambda$  defined in Sec. 2.5, which is a free parameter with dimensions  $\text{GeV}^{-1}$ , according to Eq. (39). In Fig. 10 we use  $\lambda = 1000 \text{ GeV}^{-1}$ . The visi-

$\tilde{g}$	0.7g	$g \equiv g_{D\bar{D}}$	1.3g
Pole 1	—	$3741.2 - i18.5$	$3741.0 - i9.5$
Pole 2	$3773.5 - i5.5$	$3776.8 - i12.3$	$3784.9 - i17.2$

**Table 4** Variation in the poles position with the coupling  $\tilde{g}$ , for parameters in Table 1 (cf. Fig. 9).

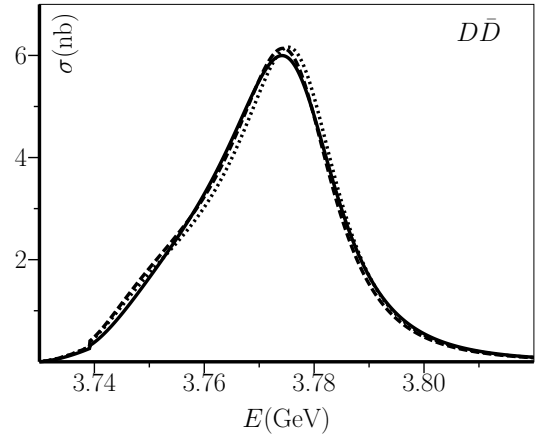


**Fig. 10** Final state rescattering effect using parameters in Table 1, and rescattering parameter  $\lambda = 1000 \text{ GeV}^{-1}$  (cf. Eq. (39)). Solid line: no rescattering, i.e. loop-function in Eq. (22). Dotted line: rescattering using Eq. 40. Dashed line: rescattering using Eq. 41.

ble effect, comparatively with the result without rescattering, consists in pronouncing slightly the asymmetry of the resonance, which might be an improvement to the fit, but that we cannot disentangle with the current experimental precision. For larger  $\lambda$  values, the cross section becomes inadequate to describe the data, from where we conclude that the rescattering of final states plays a minor role in the dynamics.

### 3.3 Estimating the size of the wave-function

The size of the  $\psi$  resonance is intrinsically related to the empirical form factor that one needs to include at the effective vertices. In the isospin limit the form factor reads  $e^{-k^2/\Lambda^2}$ , whose Fourier transform is proportional to  $e^{-\Lambda^2 r^2/4}$ , from where the variance  $\sigma^2$  of the distribution in the coordinate space is given by  $\sigma^2 = 2/\Lambda^2$ . Here, we would like to understand if the value  $\Lambda \simeq 273$  MeV found in our fit is physically meaningful. Namely, it is a factor two smaller than the value found in Ref. [9] for the light scalar kaonic system. For this purpose, we estimate the size of  $\psi$  by employing the Schrödinger

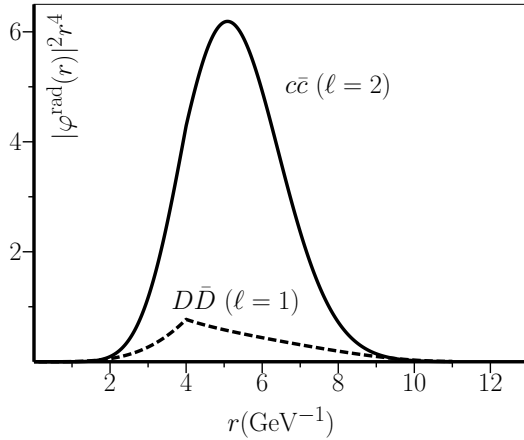


**Fig. 11**  $|\varphi^{\text{rad}}(r)|^2 r^4$  distribution for the system  $c\bar{c}-D\bar{D}$ , computed within the model in Ref. [42], with parameters  $r_0 = 4$   $\text{GeV}^{-1}$  and coupling 0.8 (see Ref. [42] for definitions).

model defined in Ref. [42], to which we refer for all technical details.

We consider the coupled system  $c\bar{c}-D\bar{D}$ , where  $c\bar{c}$  is a charmonium system with quantum numbers  $^3S_1$ ,  $L_J = ^3D_1$ , and  $D\bar{D}$  is a meson-meson decay channel. The model in Ref. [42] has two parameters that we tune to obtain the pole of  $\psi$ . For each complex energy, the root mean square (r.m.s.) is given by

$$\sqrt{\langle r^2 \rangle} = \int_0^\infty |\varphi^{\text{rad}}(r)|^2 r^4 dr \quad (50)$$

$$= \int_0^\infty \left( |\varphi_{c\bar{c}}^{\text{rad}}(r)|^2 + |\varphi_{D\bar{D}}^{\text{rad}}(r)|^2 \right) r^4 dr \quad (51)$$

where the quantity  $\varphi^{\text{rad}}(r)$  is the radial wave-function. We find a r.m.s. value that varies, respectively, within  $4.54 \text{ GeV}^{-1}$  ( $\simeq 0.97 \text{ fm}$ ) and  $4.91 \text{ GeV}^{-1}$  ( $\simeq 0.90 \text{ fm}$ ). The seemingly large value for a heavy system is essentially due to the fact that the  $\psi(3770)$  is dominantly a  $d$ -wave. In Fig. 11 we plot the  $|\varphi^{\text{rad}}(r)|^2 r^4$  distribution for the two component wave-function. If we compare it to the standard deviation, i.e.

$$\Lambda \simeq \frac{\sqrt{2}}{\sigma} \equiv \frac{\sqrt{2}}{\sqrt{\langle r^2 \rangle}}, \quad (52)$$

we get a cutoff between  $288 < \Lambda < 311 \text{ MeV}$ , pretty close to the parameter  $\Lambda$  of our fit. The range of r.m.s. values we get is yet comparable with the  $r_0$  parameter in Ref. [12] for the same system, found to be  $r_0 = 0.962$ , the physical meaning of it being an average distance for emerging the meson pair from the interaction region, which is consistent with our interpretation.

#### 4 Summary and Conclusions

Vector mesons can be produced by a single virtual photon, hence they play a crucial role in the experimental study of QCD. In the light sector, ground-state vector mesons represent the lightest (almost) ideal nonet of  $q\bar{q}$  states with a mass of about  $2m^*$ , where  $m^*$  is the constituent quark mass of about 350 MeV. The production and decays of the  $\rho$ ,  $\omega$  and  $\phi$  meson in  $e^+e^-$  improved our understanding of QCD, see e.g. the theoretical review in Ref. [43], where also the so-called Vector Meson Dominance is presented, and the experimental review in Ref. [44]. Moreover, also excited vector states below 2 GeV exist (see Ref. [45] and references therein). The renowned charmonium vector state  $J/\psi$  opened a new era in hadron physics and is one of the best studied resonances (cf. [2]).

Here, we have focused on an orbital excitation of  $J/\psi$ , the meson  $\psi(3370)$ , whose mass lies just above the  $D\bar{D}$  threshold. For this reason, this resonance is extremely interesting. The cross-section  $e^+e^- \rightarrow \psi \rightarrow D\bar{D}$  encloses nonperturbative phenomena nearby the OZI-allowed open decay channel  $D\bar{D}$ . The production and decay to all hadrons shows evidence of a deformation on the left energy side of the resonance [8] that is not obvious in the  $D\bar{D}$  cross section only, as we have verified from our line-shape results. Within the presented nonperturbative effective Lagrangian model, with only one bare  $\bar{c}c$  seed state  $\psi$  at the start, we found not only one, but two poles underlying the enhancement: a standard seed pole, very close to the one determined by BES in Ref. [8], and a broader dynamically generated pole at lower energy, being an additional companion pole (see Eqs. (47) and (49) for the numerical values). The existence of the second pole gives us a new insight over the relevance of dynamical effects, here represented by the  $D\bar{D}$  coupled-channel loops, besides the expected kinematical interferences.

The width of about 24 MeV to channel  $D\bar{D}$ , that we obtain from the first pole, is consistent with the experimental measurements to this channel, and with the branching fraction estimated to be about 85% in Ref. [46], considering that measurements of the width in decays to all hadrons are a few MeV higher (cf. Ref. [2]). A natural outlook is the inclusion of the many OZI-suppressed hadronic decay channels and the study of their influence on the pole position and on the line-shape. Other effects, such as final state rescattering and the contribution of the tail of the  $\psi(2S)$  to the amplitude, are expected to improve the results, but we predict their influence to be small. Better statistics in the data may disentangle such variations. A related topic is the evaluation of mixing with the vector glueball,

whose mass is predicted to be at about 3.8 GeV by lattice QCD [47] (for a general introduction on glueballs, see Ref. [48]). Namely, mixing effects can be interesting to study the OZI suppressed decays (for decays of the glueball see Ref. [47]).

Finally, the same theoretical approach used in this work, and tested on the well-known resonance  $\psi(3770)$ , can be applied to other resonances whose nature is not yet clarified, the so-called  $X$ ,  $Y$ , and  $Z$  states [49]. While for the  $\psi(3770)$  the additional pole is responsible for a deformation on the left side but not for an additional peak, a coupling constant which is larger could generate a peak, as shown in Fig. 9, and in Ref. [28] as an explanation of the resonance  $a_0(980)$  in the light scalar sector. It is well possible that some of the  $X$  and  $Y$  resonances arise as companion poles due to a strong coupling of a standard charmonium seed state to lighter mesonic resonances. The strong dressing of the original state with meson-meson clouds generates new poles and new peaks. An intriguing possibility is that the additional peak arises at higher energy than the seed state, see Ref. [50] for the phenomenological description of this phenomenon in the light sector. Namely, if new decay channels open just above the mass of the seed state, companion poles and related peaks may arise on the right side.

## Acknowledgements

We thank to G. Rupp and E. van Beveren for useful discussions. This work was supported by the *Polish National Science Center* through the project OPUS no. 2015/17/B/ST2/01625.

## Appendix A: Full Lagrangian

The complete form of the Lagrangian used in this work is given by:

$$\mathcal{L}_0 = -\frac{1}{4}V_{\mu\nu}V^{\mu\nu} + \frac{1}{2}m_\psi^2\psi_\mu\psi^\mu \quad (\text{A.1})$$

$$+ \frac{1}{2}\left(\partial_\mu D^+ \partial^\mu D^- - m_{D^+}^2 D^+ D^-\right) \quad (\text{A.2})$$

$$+ \frac{1}{2}\left(\partial_\mu D^0 \partial^\mu \bar{D}^0 - m_{D^0}^2 D^0 \bar{D}^0\right) \quad (\text{A.3})$$

$$+ \sum_{l=e,\mu,\tau} \bar{\Psi}_l (i\gamma^\mu \partial_\mu - m_l) \Psi_l, \quad (\text{A.4})$$

$$\mathcal{L}_{full} = \mathcal{L}_0 + \mathcal{L}_{\psi D\bar{D}} + \mathcal{L}_{\psi l^+ l^-}, \quad (\text{A.5})$$

where in the first line the definition  $V_{\mu\nu} = \partial_\mu \psi_\nu - \partial_\nu \psi_\mu$  has been implemented, and the interacting terms in Eq. (A.5) are given by Eqs. (1) and (27).

## Appendix B: Details of the Loop Function

Here, we derive the propagator of the vector resonance  $\psi$  dressed by  $D\bar{D}$  loops. The considerations are, however, general and can be applied to loops of each vector state. Using the shortening notations

$$\int_q \equiv \int \frac{d^4 q}{(2\pi)^4}, \quad (\text{B.6})$$

$$\mathcal{D} \equiv [(q + \frac{p}{2})^2 - m^2 + i\varepsilon][(q - \frac{p}{2})^2 - m^2 + i\varepsilon], \quad (\text{B.7})$$

we decompose the tensor loop contribution  $\Sigma_{\mu\nu}(s, m)$  in transverse and longitudinal parts:

$$\begin{aligned} \Sigma_{\mu\nu}(s, m) &= i \int_q \frac{4q_\mu q_\nu f_A^2(s)}{\mathcal{D}} \\ &= \left(-g_{\mu\nu} + \frac{p_\mu p_\nu}{p^2}\right) \Sigma + p_\mu p_\nu \Sigma_L. \end{aligned}$$

Then, multiplying by  $g^{\mu\nu}$  and  $p^\mu p^\nu$ , respectively, we get:

$$g^{\mu\nu} \Sigma_{\mu\nu}(s, m) = i \int_q \frac{4q^2 f_A^2(s)}{\mathcal{D}} = -3\Sigma + p^2 \Sigma_L, \quad (\text{B.8})$$

$$p^\mu p^\nu \Sigma_{\mu\nu}(s, m) = i \int_q \frac{4(p \cdot q)^2 f_A^2(s)}{\mathcal{D}} = p^4 \Sigma_L, \quad (\text{B.9})$$

out of which we find, in the rest-frame of the decaying particle,  $p = (E, \mathbf{0})$ , where  $E$  is the running mass of the  $\psi(3770)$ :

$$\Sigma(s, m) = \frac{1}{3} \left(-g^{\mu\nu} + \frac{p^\mu p^\nu}{p^2}\right) \Sigma_{\mu\nu}(s) \quad (\text{B.10})$$

$$= -\frac{4}{3}i \int_q \frac{\mathbf{q}^2 f_A^2(s)}{\mathcal{D}}. \quad (\text{B.11})$$

It is clear that  $\Sigma$  is the scalar quantity entering in the denominator of the loop. Namely, its imaginary part reads:

$$\text{Im } \Sigma(s, m) = E \frac{4}{3} \frac{|\mathbf{k}_f|^3}{8\pi E^2} f_A^2(E^2) = E \Gamma(E, m), \quad (\text{B.12})$$

as it should. Similarly, for the sum of the two contributions, one has:

$$\Pi(s) = \frac{1}{3} \left(-g^{\mu\nu} + \frac{p^\mu p^\nu}{p^2}\right) \Pi_{\mu\nu}(s), \quad (\text{B.13})$$

$$p^\mu p^\nu \Pi_{\mu\nu}(s, m) = p^4 \Pi_L. \quad (\text{B.14})$$

Indeed, an explicit resummation of the full propagator shows that

$$\begin{aligned}
\Delta_{\mu\nu}(p) &= G_{\mu\nu}(p) + G_{\mu\mu'}(p)\Pi_{\mu'\nu'}(p)G_{\nu'\nu}(p) + \dots \\
&= G_{\mu\nu}(p) + \left( \frac{-g_{\mu\mu'} + \frac{p_\mu p_{\mu'}}{p^2}}{p^2 - m_\psi^2} - \frac{p_\mu p_\nu}{p^2 m_\psi^2} \right) \times \\
&\quad \left[ \left( -g_{\mu'\nu'} + \frac{p_{\mu'} p_{\nu'}}{p^2} \right) \Pi + p_{\mu'} p_{\nu'} \Pi_L \right] \times \\
&\quad \left( \frac{-g_{\nu'\nu} + \frac{p_{\nu'} p_\nu}{p^2}}{p^2 - m_\psi^2} - \frac{p_{\nu'} p_\nu}{p^2 m_\psi^2} \right) + \dots \\
&= \frac{-g_{\mu\nu} + \frac{p_\mu p_\nu}{p^2}}{p^2 - m_\psi^2} - \frac{p_\mu p_\nu}{p^2 m_\psi^2} + \frac{-g_{\mu\nu} + \frac{p_\mu p_\nu}{p^2}}{\left( p^2 - m_\psi^2 \right)^3} \Pi \\
&\quad - \frac{p_\mu p_\nu}{p^2 M_0^2} \frac{\Pi_L}{m_\psi^2} + \dots \\
&= \frac{-g_{\mu\nu} + \frac{p_\mu p_\nu}{p^2}}{p^2 - m_\psi^2 + \Pi} - \frac{p_\mu p_\nu}{m_\psi^2 - \Pi_L^2}, \tag{B.15}
\end{aligned}$$

where we have used

$$G_{\mu\nu}(p) = \frac{-g_{\mu\nu} + \frac{p_\mu p_\nu}{M_0^2}}{p^2 - m_\psi^2} = \frac{-g_{\mu\nu} + \frac{p_\mu p_\nu}{p^2}}{p^2 - m_\psi^2} - \frac{p_\mu p_\nu}{p^2 m_\psi^2}. \tag{B.16}$$

The final result reads

$$\Delta_{\mu\nu}(p) = \frac{-g_{\mu\nu} + \frac{p_\mu p_\nu}{p^2}}{p^2 - m_\psi^2 + \Pi} - \frac{p_\mu p_\nu}{m_\psi^2 - \Pi_L^2}, \tag{B.17}$$

where it is evident that the first part contains the properties of the unstable state.

## References

1. P.A. Rapidis *et al.*, *Observation of a Resonance in  $e^+e^-$  Annihilation Just above Charm Threshold*, Phys. Rev. Lett. **39**, 526 (1977).
2. C. Patrignani *et al.* (Particle Data Group), Chin. Phys. C **40**, 100001 (2016).
3. R. Christov *et al.* (Belle Collaboration), *Observation of  $B^+ \rightarrow \psi(3770)K^+$* , Phys. Rev. Lett. **93**, 051803 (2004).
4. M. Ablikim, *et al.* (BES Collaboration), *Measurements of the Branching Fractions for  $\psi(3770) \rightarrow D^0\bar{D}^0, D^+D^-, D\bar{D}$ , and the Resonance Parameters of  $\psi(3770)$  and  $\psi(2S)$* , Phys. Rev. Lett. **97**, 121801 (2006).
5. B. Aubert, *et al.* (BABAR Collaboration), *Study of the exclusive initial-state-radiation production of the  $D\bar{D}$  system*, Phys. Rev. D **76**, 111105 (R) (2007).
6. M. Ablikim, *et al.* (BES Collaboration), *Measurements of the line-shapes of  $D\bar{D}$  production and the ratio of production rates of  $D^+D^-$  and  $D^0\bar{D}^0$  in  $e^+e^-$  annihilation at  $\psi(3770)$* , Phys. Lett. B **668**, 263 (2008).
7. V.V. Anashin *et al.*, *Measurement of  $\psi(3770)$  parameters*, Phys. Lett. B **711**, 292 (2012).
8. M. Ablikim, *et al.* (BES Collaboration), *Anomalous Line Shape of the Cross Section for  $e^+e^- \rightarrow \text{Hadrons}$  in the Center-of-Mass Energy Region between 3.650 and 3.872 GeV*, Phys. Rev. Lett. **101**, 102004 (2008).
9. T. Wolkanowski, M. Sołtysiak, and F. Giacosa,  *$K_0^*(800)$  as a companion pole of  $K_0^*(1430)$* , Nuc. Phys. B **909**, 418 (2016).
10. N.N. Achasov and G.N. Shestakov, *Line shape of  $\psi(3770)$  in  $e^+e^- \rightarrow D\bar{D}$* , Phys. Rev. D **86**, 114013 (2012).
11. N.N. Achasov and G.N. Shestakov, *Description of the  $\psi(3770)$  resonance interfering with the background*, Phys. Rev. D **87**, 057502 (2013).
12. E. van Beveren and G. Rupp, *Production of hadron pairs in  $e^+e^-$  annihilation near the  $K^+K^-, D\bar{D}, B\bar{B}$ , and  $\Lambda_c^+\Lambda_c^-$  thresholds*, Phys. Rev. D **80**, 074001 (2009).
13. R. Wang, X. Cao, and X.R. Chen, *The  $R_{uds}$  value in the vicinity of  $\psi(3770)$  state*, Phys. Lett. B **747**, 321 (2015).
14. M. Ablikim *et al.* (BES Collab.), *Measurements of the cross sections for  $e^+e^- \rightarrow \text{hadrons}$  at 3.650, 3.6648, 3.773 GeV and the branching fraction for  $\psi(3770) \rightarrow \text{non-}D\bar{D}$* , Phys. Lett. B **641**, 145 (2006).
15. D. Besson *et al.* (CLEO Collaboration), *Measurement of  $\sigma(e^+e^- \rightarrow \psi(3770)\text{hadrons})$  at  $E_{c.m.} = 3773$  MeV*, Phys. Rev. Lett. **96**, 092002 (2006).
16. A.G. Shamov and K.Yu. Todyshev, *Analysis of BaBar, Belle, BES-II, CLEO and KEDR data on  $\psi(3770)$  line shape and determination of the resonance parameters*, Phys. Lett. B **769**, 187 (2017).
17. H.B. Li, X.S. Qin, and M.Z. Yang, *Study of the branching ratio of  $\psi(3770) \rightarrow D\bar{D}$  in  $e^+e^- \rightarrow D\bar{D}$  scattering*, Phys. Rev. D **81**, 011501(R) (2010).
18. G. Li, X.H. Liu, Q. Wang, and Q. Zhao, *Further understanding of the non- $D\bar{D}$  decays of  $\psi(3770)$* , Phys. Rev. D **88**, 014010 (2013).
19. X. Liu, B. Zhang, and X.Q. Li, *The puzzle of excessive non- $D\bar{D}$  component of the inclusive  $\psi(3770)$  decay and the long-distant contribution*, Phys. Lett. B **675**, 441 (2009).
20. M. Ablikim *et al.*, *Study of  $e^+e^- \rightarrow p\bar{p}\pi^0$  in the vicinity of the  $\psi(3770)$* , Phys. Rev. D **90**, 032007 (2014).
21. H. Xu, J.J. Xie, and X. Liu, *Implications of the observed  $e^+e^- \rightarrow p\bar{p}\pi^0$  for studying  $p\bar{p} \rightarrow \psi(3770)\pi^0$* , Eur. Phys. J. C **76**, 192 (2016).
22. J. Haidenbauer and G. Krein,  *$\psi(3770)$  resonance and its production in  $p\bar{p} \rightarrow D\bar{D}$* , Phys. Rev. D **91**, 114022 (2015).
23. M. F. M. Lutz *et al.* [PANDA Collaboration], *Physics Performance Report for PANDA: Strong Interaction Studies with Antiprotons*, arXiv:0903.3905 [hep-ex].
24. S. Coito and F. Giacosa, *Formation and Deformation of the  $\psi(3770)$* , arXiv: 1708.02041 [hep-ph].
25. D. Gammermann and E. Oset, *Hidden charm dynamically generated resonances and the  $e^+e^- \rightarrow J/\psi D\bar{D}, J/\psi D\bar{D}$  reactions*, Eur. Phys. J. A **36**, 189 (2008).
26. F. Giacosa and G. Pagliara, *Spectral functions of scalar mesons*, Phys. Rev. C **76**, 065204 (2007).
27. F. Giacosa and G. Pagliara, *Spectral function of a scalar boson coupled to fermions* Phys. Rev. D **88**, 025010 (2013).
28. T. Wolkanowski, F. Giacosa and D. H. Rischke,  *$a_0(980)$  revisited*, Phys. Rev. D **93**, 014002 (2016).
29. M. Boglione and M. R. Pennington, *Dynamical generation of scalar mesons*, Phys. Rev. D **65**, 114010 (2002).
30. N. A. Tornqvist, *Understanding the scalar meson  $q$  anti- $q$  nonet*, Z. Phys. C **68**, 647 (1995).
31. E. van Beveren, T. A. Rijken, K. Metzger, C. Dullemond, G. Rupp, and J. E. Ribeiro, *A Low Lying Scalar Meson Nonet in a Unitarized Meson Model*, Z. Phys. C **30**, 615 (1986)

- 
32. G.Y. Chen and Q. Zhao, *Study of the anomalous cross-section lineshape of  $e^+e^- \rightarrow D\bar{D}$  at  $\psi(3770)$  with an effective field theory*, Phys. Lett. B **718**, 1369 (2013).
33. Y.J. Zhang, and Q. Zhao, *Lineshape of  $\psi(3770)$  and low-lying vector charmonium resonance parameters in  $e^+e^- \rightarrow D\bar{D}$* , Phys. Rev. D **81**, 034011 (2010).
34. R. D. Bowler and M. C. Birse, *A Nonlocal, covariant generalization of the NJL model*, Nucl. Phys. A **582**, 655 (1995)
35. A. Faessler, T. Gutsche, M. A. Ivanov, V. E. Lyubovitskij and P. Wang, *Pion and sigma meson properties in a relativistic quark model*, Phys. Rev. D **68**, 014011 (2003).
36. F. Giacosa, T. Gutsche and A. Faessler, *A Covariant constituent quark gluon model for the glueball-quarkonia content of scalar - isoscalar mesons*, Phys. Rev. C **71**, 025202 (2005)
37. M. Soltysiak and F. Giacosa, *A covariant nonlocal Lagrangian for the description of the scalar kaonic sector*, Acta Phys. Polon. Supp. **9**, 467 (2016).
38. J. Schneitzer, T. Wolkanowski and F. Giacosa, *The role of the next-to-leading order triangle-shaped diagram in two-body hadronic decays*, Nucl. Phys. B **888**, 287 (2014)
39. F. Giacosa, *Non-exponential decay in quantum field theory and in quantum mechanics: the case of two (or more) decay channels*, Found. Phys. **42**, 1262 (2012).
40. J. R. Pelaez and A. Rodas, *The non-ordinary Regge behavior of the  $K_0^*(800)$  or  $\kappa$ -meson versus the ordinary  $K_0^*(1430)$* , Eur. Phys. J. C **77**, 431 (2017).
41. J. R. Pelaez and A. Rodas, *Pion-kaon scattering amplitude constrained with forward dispersion relations up to 1.6 GeV*, Phys. Rev. D **93**, 074025 (2016).
42. S. Coito, *Radially excited axial mesons and the enigmatic  $Z_c$  and  $Z_b$  in a coupled-channel model*, Phys. Rev. D **94**, 014016 (2016).
43. H. B. O'Connell, B. C. Pearce, A. W. Thomas and A. G. Williams,  *$\rho - \omega$  mixing, vector meson dominance and the pion form-factor*, Prog. Part. Nucl. Phys. **39**, 201 (1997).
44. G. Amelino-Camelia *et al.*, *Physics with the KLOE-2 experiment at the upgraded DA $\phi$ NE*, Eur. Phys. J. C **68**, 619 (2010).
45. M. Piotrowska, C. Reisinger and F. Giacosa, *Strong and radiative decays of excited vector mesons and predictions for a new  $\phi(1930)$  resonance*, Phys. Rev. D **96**, 054033 (2017).
46. M. Ablikim *et al.* (BES Collaboration), *Direct measurements of the cross sections for  $e^+e^- \rightarrow \text{hadrons}|_{\text{non-}D\bar{D}}$  in the range from 3.65 to 3.87 GeV and the branching fraction for  $\psi(3770) \rightarrow \text{non-}D\bar{D}$* , Phys. Lett. B **659**, 74 (2008).
47. Y. Chen *et al.*, *Glueball spectrum and matrix elements on anisotropic lattices*, Phys. Rev. D **73**, 014516 (2006).
48. W. Ochs, *The Status of Glueballs*, J. Phys. G **40**, 043001 (2013); V. Mathieu, N. Kochelev and V. Vento, *The Physics of Glueballs*, Int. J. Mod. Phys. E **18**, 1 (2009); V. Crede and C. A. Meyer, *The Experimental Status of Glueballs*, Prog. Part. Nucl. Phys. **63**, 74 (2009).
49. H. X. Chen, W. Chen, X. Liu and S. L. Zhu, *The hidden-charm pentaquark and tetraquark states*, Phys. Rept. **639**, 1 (2016).
50. V. R. Debastiani, F. Aceti, W. H. Liang and E. Oset, *Revising the  $f_1(1420)$  resonance*, Phys. Rev. D **95**, 034015 (2017).